Research Article

For reprint orders, please contact: reprints@futuremedicine.com

Nanomedicine

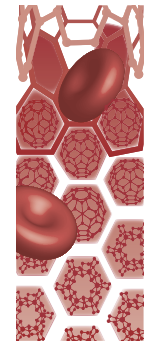

Neutrophil and endothelial cell membranes coassembled roflumilast nanoparticles attenuate myocardial ischemia/reperfusion injury

Ying Tan[‡,1], Xun Wang[‡,2], Yu Gu[‡,1], Xue Bao[1], He Lu[3], Xuan Sun[1], Lina Kang*[,1] & Biao Xu**[,1]

[1]Department of Cardiology, Nanjing Drum Tower Hospital, Affiliated Hospital of Medical School, Nanjing University, Nanjing, Jiangsu, 210000, China

[2]Department of Urology, Nanjing Drum Tower Hospital, Affiliated Hospital of Medical School, Nanjing University, Nanjing, Jiangsu, 210000, China

[3]Department of Cardiology, Nanjing Drum Tower Hospital, Clinical College of Nanjing University of Chinese Medicine, Nanjing, Jiangsu, 210000, China

*Author for correspondence: kanglina@nju.edu.cn

**Author for correspondence: xubiao62@nju.edu.cn

‡Authors contributed equally

Aim: This study aimed to develop biomimetic nanoparticles (NPs) of roflumilast (ROF) for attenuating myocardial ischemia/reperfusion (MI/R) injury. **Materials & methods:** We synthesized biomimetic ROF NPs and assembled ROF NPs in neutrophil and endothelial cell membranes (NE/ROF NPs). The physical properties of NE/ROF NPs were characterized and biological functions of NE/ROF NPs were tested *in vitro*. Targeting characteristics, therapeutic efficacy and safety of NE/ROF NPs were examined in mice model of MI/R. **Results:** NE/ROF NPs exhibited significant anti-inflammatory and antiadhesion effects. Meanwhile, they was effective in reducing MI/R injury in mice. Furthermore, NE/ROF NPs exhibited stronger targeting capabilities and demonstrated good safety. **Conclusion:** NE/ROF NPs may be a versatile biomimetic drug-delivery system for attenuating MI/R injury.

First draft submitted: 27 October 2023; Accepted for publication: 22 January 2024; Published online: 1 March 2024

Keywords: biomimetic NPs • endothelial cell • myocardial ischemia/reperfusion injury • neutrophil • roflumilast

Acute myocardial infarction (AMI) is the most severe clinical presentation of coronary artery disease [1,2]. AMI is divided into ST-elevation myocardial infarction (MI) (STEMI) and non-ST-elevation MI [3]. A published study found a 23.3% prevalence of AMI in 19,781 patients with coronary artery disease [4]. More than 3 million people develop STEMI each year, and more than 4 million represent STEMI pathology [3]. Timely and complete reperfusion after STEMI is the most effective intervention for rescuing the ischemic heart [5]. However, while reperfusion therapy demonstrates overall efficacy, it also leads to secondary injury known as myocardial ischemia/reperfusion (MI/R) injury. Consequently, microvascular dysfunction and excessive inflammatory responses occur following reperfusion, including neutrophil aggregation and release of cytotoxic products, which further aggravate cardiomyocyte death and ultimately progress to heart failure [6,7]. So far, there is no effective strategy for the clinical prevention and treatment of MI/R injury. Current studies have shown that inhibition of neutrophils can reduce MI/R injury, reduce myocardial infarct size and improve the clinical prognosis of AMI [8,9]. This finding has led scholars to focus on the immune cells involved in the inflammatory response following MI/R. Thus, it is imperative to develop effective therapies or drugs to reduce MI/R injury.

PDE4, a family of enzymes that hydrolyze cAMP, is involved in inflammation, neuronal activation and cell proliferation [5]. PDE4 consists of four subtypes, PDE4A–D, highly expressed in the brain, cardiovascular tissue, smooth muscle and keratinocytes [10]. PDE4B plays a crucial role in MI/R injury by mediating neutrophil–endothelium interactions and neutrophil infiltration [5]. Inhibiting PDE4B not only reduces cardiomyocyte death but also alle-

viates microvascular obstruction, thus playing a dual cardiac protective role in MI/R injury [5]. Roflumilast (ROF), a selective PDE4 inhibitor, acts on PDE4B with an IC_{50} of 0.7 nM and has been approved for the treatment of severe chronic obstructive pulmonary disease due to its potent anti-inflammatory and immunomodulatory properties [11,12]. Previous studies have demonstrated that ROF prevents neuronal damage induced by ischemic stroke [13] and protects cardiomyocytes from nitric oxide (NO)-induced apoptosis [14]. Recent studies have also shown that ROF can reduce myocardial infarct size after MI/R injury [5,15]. Previous studies have demonstrated ROF alleviated MI/R in rats and attenuated hypoxia/reoxygenation-induced oxidative stress, inflammatory response and mitochondrial damage in H9c2 cells by activating the AMPK signaling pathway [15]. ROF was also proven to protect cardiomyocytes against nitric oxide (NO)-induced apoptosis via activation of PKA and Epac dual pathways [14]. However, common side effects such as diarrhea, weight loss and headaches, as well as serious side effects such as atrial fibrillation, limit the efficacy of ROF [16]. Additionally, the high frequency and complex time point of administration restrict the application of ROF in AMI. Therefore, an efficient targeted delivery system is required to enhance the efficacy of ROF and minimize adverse effects.

Traditional drugs cannot achieve the expected therapeutic effect on diseases due to poor pharmacokinetics, low permeability, rapid clearance by the body and obvious cytotoxicity. Nanoparticles (NPs) have the characteristics of tiny size (1–1000 nm), strong targeting and lengthy circulation time [17,18]. Cell membrane-coated NPs have emerged as an important tool for topical drug delivery to affected tissues in recent years due to characteristics of low immunogenicity, short half-life, low toxicity and innate targeting due to specific biological activities inherited from the source cells [19,20]. Commonly used NPs mainly include polymeric NPs (natural polysaccharides and synthetic polymers), lipid-based NPs and inorganic NPs [21,22]. Immune cells are often utilized in coating NPs to create biomimetic nanodrug delivery systems, benefiting from the cell membrane proteins that offer a wide range of activities. These activities include prolonged blood circulation, enhanced targeting through antigen recognition, improved cell interaction, gradual drug release and reduced *in vivo* toxicity [23–25]. At present, poly(lactic-co-glycolic acid) (PLGA) is the most commonly used NPs carrier because of its excellent biocompatibility, biodegradability and relatively long retention time in the circulation, and the preparation method of PLGA microspheres is relatively mature [26,27]. The applications of Förster resonance energy transfer (FRET), surface plasmon resonance and single-molecule techniques are to measure specific molecular interactions taking place in biology systems [28–30].

Neutrophils, the earliest immune cells to infiltrate the infarcted myocardial area following myocardial infarction, interact with endothelial cells (ECs) through increased adhesion molecules, such as VCAM-1 or ICAM-1 [31]. These markers facilitate the adhesion of immune cells to sites of inflammation [32]. By encapsulating therapeutic NPs within the membranes of naturally derived neutrophils, the lifespan of NPs in peripheral blood is extended, allowing for enhanced interaction between NPs and injured tissues [33]. Taking advantage of inflammation as a targeting cue, various nanodelivery systems have been designed to target upregulated markers, including VCAM-1 and ICAM-1 [34]. This approach has been utilized for the treatment of diseases such as cancer and cardiovascular disease [35].

In this study, we developed polymeric cores composed of PLGA loaded with ROF. These cores were then coated with naturally derived neutrophil and endothelial cell membranes (NE), resulting in NE/ROF NPs. The fusion of NE offers a significant advantage as the two membranes can mutually benefit each other [33]. Neutrophil membranes possess the ability to absorb toxins, suppress inflammatory cytokines and facilitate targeted delivery to inflamed areas of the heart. On the other hand, EC membranes competitively bind to neutrophils by inheriting multiple receptors from their 'parent' ECs. This binding impedes neutrophil adhesion to inflamed endothelium, reduces neutrophil infiltration in the area of reperfusion injury and enhances the therapeutic effects of NPs. Subsequently, we investigated the therapeutic efficacy and effects of NE/ROF NPs both *in vitro* and *in vivo*.

Materials & methods

Isolation of neutrophil & endothelial cell membranes

Cellular membranes of murine neutrophils and aortic ECs were extracted by the hypotonic lysis method [36,37]. Briefly, the neutrophil or EC suspension from six 100 mm dishes was collected and centrifuged at low speed (900 r.p.m., 5 min) at 4°C. The resulting pellet was resuspended in precooled phosphate-buffer solution (PBS) and centrifuged again. Then, 2 ml of precooled hypotonic lysate solution (10 mM Tris-HCl pH = 8.0, 1 mM KCl, 1.5 mM $MgCl_2$ and 1 mM phenylmethanesulfonyl fluoride) was added, and the solution was placed in an ice bath for 15 min. The cell suspension was then repeatedly disrupted by rapid freezing and thawing for four to five cycles with liquid nitrogen followed by room temperature. The supernatant was then collected by

low-speed centrifugation (850× g, 10 min) at 4°C and centrifuged again (15,000× g, 30 min), and the precipitate was regarded as cell membrane debris. Finally, the membranes were resuspended with an appropriate amount of hypotonic lysate (storage at -20°C), and the protein concentration was determined using a bicinchoninic acid (BCA) kit (Thermo Fisher Scientific, MA, USA; storage at -20°C).

Preparation of roflumilast nanoparticles

ROF NPs were prepared via the nanoprecipitation method as previously described with a slight modification [38,39]. Briefly, ROF (1.0 mg, MedChemExpress, NJ, USA) and PLGA (10 mg) were dissolved in dimethyl sulfoxide (DMSO; 1 ml). The mixture was precipitated by adding 4 ml of water dropwise with gentle stirring. Then, free ROF and DMSO were removed by dialysis (molecular weight cutoff of 3500 Da). The ROF NPs solution was stored at 4°C. DiI-labeled NPs were prepared for *in vitro* and *in vivo* experiments using the above method (0.1 wt% DiI).

Preparation of neutrophil and endothelial cell membranes coassembled roflumilast NPs

To harvest membrane vesicles from neutrophils and ECs, the extracted membranes were first sonicated for 20 min and then extruded through a membrane filter with a pore size of 400 nm. The compression was repeated more than ten times. Neutrophil and endothelial membrane vesicles were then mixed in a 1:1 ratio with ROF NPs (membrane protein-to-polymer ratio of 1:1), sonicated and extricated through a membrane filter with a pore size of 200 nm. After undergoing more than ten rounds of squeezing, an ultrasound was performed for 5 min using an ultrasound probe [36].

Characterization of neutrophil and endothelial cell membranes coassembled roflumilast NPs

The hydrodynamic diameter and zeta potential of neutrophil membranes, ROF NPs and [NE]/ROF NPs were determined by using dynamic light scattering (DLS) NanoSight (Malvern Panalytical, Malvern, UK). The morphology was determined using transmission electron microscopy (FEI Tecnai F20, OR, USA).

The formulated ROF NPs were dissolved in DMSO and the absorbance was measured using a spectrophotometer (Tecan, Mannedorf, Switzerland) at a wavelength of 290 nm (refer to the result of Supplementary Figure 1). According to the preestablished standard curve of ROF in DMSO (Supplementary Figure 1), the drug-loading efficiency (LE) and drug-encapsulation efficiency (EE) were calculated previously described as follows [36,37]:

$$LE = \frac{M\,(ROF)}{M\,(PLGA) + M\,(ROF)} \times 100\%$$

$$EE = \frac{M\,(ROF)}{M\,(added)} \times 100\%$$

where M(ROF) is the mass of ROF loaded in the NPs, M(PLGA) is the mass of polymer in the formulation, and M(added) is the mass of ROF added.

ROF release from NPs was measured using dialysis bags. In brief, ROF NPs and [NE]/ROF NPs solutions (2 mg/ml, 1 ml each) were added to disposable dialysis bags (molecular weight cut-off [MWCO]: 3500 Da, Thermo Fisher Scientific, MA, USA). The dialysis bags were then immersed in 10 ml of PBS (release medium, pH 7.4) at 37°C. At various intervals, 1 ml of release medium was collected for analysis and replaced with an equal volume of fresh PBS at 37°C [36]. The cumulative release of ROF was measured at 290 nm using a UV/visible spectrophotometer (Tecan).

The fusion process of neutrophil membranes and EC membranes was determined using FRET method [40]. A FRET dye pair, 3,3′-dioctadecyloxacarbocyanine perchlorate (DiO) (Beyotime, Shanghai, China) and 1,1′-dioctadecyl-3,3,3′,3′-tetramethylindocarbocyanine perchlorate (Dil) (Beyotime) (0.1%, w:w), were added to neutrophil membranes. EC membranes were then added to DiO- and Dil-labeled neutrophil membranes, sonicated and extruded, and sample fluorescence spectra at 400 nm were measured using a fluorescence spectrometer (Tecan).

Expressions of neutrophils, ECs and membrane-associated proteins were detected using Coomassie blue staining and western blot (WB) [33]. In brief, neutrophils, ECs, EC membranes and NE coassembled NPs (NE/NPs) were lysed in lysis buffer for 30 min on ice. The supernatant was collected by centrifugation at 12,000× g for 10 min.

Then, the sodium dodecyl sulfate supernatant was mixed with the supernatant and boiled for 5 min. All samples were loaded into each well at a concentration of 20 μg protein. Gelatin was stained with Coomassie blue staining solution to obtain full imaging. For WB, all proteins were transferred to polyvinylidene difluoride membranes (Millipore, MA, USA) and blocked with 5% nonfat milk for 2 h at 37°C. Next, primary antibodies against ICAM-1 and VCAM-1 were incubated with bands overnight at 4°C, followed by incubation with secondary antibodies. Finally, specific bands were observed using an enhanced chemiluminescence detection kit, and the signals were detected with an electrochemiluminescence ECL system (Amersham ImageQuant, Amersham, UK). The WB bands were analyzed by ImageJ software.

Neutrophil and endothelial membranes were labeled with 1,1'-dioctadecyl-3,3,3',3'-tetramethylindocarbocyanine, 4-chlorobenzene sulfonate salt (DiD) and DiO, respectively, and prepared for fusion as described above. The samples were imaged using a confocal laser scanning microscope (CLSM; Leica, Hessen, Germany).

Cell culture

Mouse neutrophil cells (MNHCs) were purchased from Qingqi Biotechnology Development Co. Ltd (Shanghai, China), and mouse aortic endothelial cells (MAECs) were purchased from BeNa Culture Collection (Xinyang, China). All cells were cultured in DMEM containing 10% fetal bovine serum and cultured at 37°C in a humidified environment containing 5% CO_2 and 95% O_2.

In vitro targeting ability study

MAECs were stimulated with recombinant mouse TNF-α (50 ng/ml) for 24 h to mimic activated ECs in hearts. After coincubation of 100 μg Dil NPs and [NE]/Dil NPs with MAECs for 2 h, nuclei were stained with 6-diamidino-2-phenylindole (DAPI) (Beyotime) and visualized by CLSM.

In vitro efficacy evaluation

MNHCs were stimulated with lipopolysaccharide (LPS) (1 μg/ml) for 4 h to simulate the inflammatory response after MI/R [41], 12 h after adding ROF NPs or [NE]/ROF NPs with 1 μM ROF into culture medium according to previous studies [15]. MNHCs were collected and the Trizol method used (Vazyme Biotech Co. Ltd, Nanjing, China) to extract total intracellular RNA and obtained cDNA samples with a reverse transcriptase kit (Vazyme, Nanjing, China). The cDNA samples were diluted by a factor of ten before use. On the ABI Step, one Plus QPCR instrument (Thermo Fisher Scientific), a quantitative real-time PCR analysis of cDNA was performed using SYBR Green QPCR Master Mix (Vazyme, Nanjing, China). The sequences of PCR primers are shown in Supplementary Table 1.

MAEC was stimulated with LPS (1 μg/ml; Sigma-Aldrich, MO, USA) for 4 h to simulate endothelial dysfunction after MI/R. This was followed by the addition of ROF NPs or NE/ROF NPs with 1 μM ROF for a total of 12 h [42]. WB mentioned above was used to examine adhesion molecular proteins: ICAM-1 and VCAM-1.

Animals

All animal experimental procedures were approved by the Institutional Ethics Committee of Nanjing Drum Tower Hospital (approval no. 2021AE02005) and were performed in accordance with the guidelines outlined in the Guide for the Care and Use of Laboratory Animals published by the NIH.

Mouse model of myocardial ischemia/reperfusion

To establish the MI/R model, 8-week-old male C57BL/6 mice were used. Mice were anesthetized by inhalation of isoflurane (1.5–2%) and ventilated with room air using a ventilator. A thoracotomy was performed at the fourth intercostal space to expose the heart and left anterior descending coronary artery (LAD). LAD was ligated with 7-0 silk thread and released after 45 min to restore blood perfusion. Mice in the sham group were not ligated. Free ROF, ROF NPs and NE/ROF NPs in 0.9% sodium chloride solution at a dose of 1 mg/kg of ROF were injected via the tail vein immediately after reperfusion. The injection dose of ROF was referred to in previous studies [13]. The PBS group was injected with the same volume of PBS. Mice were euthanized at 24 h, 72 h, 3 days (d) and 7 days separately after reperfusion to allow for the collection of samples.

In vivo targeting ability study

Mice were injected with equal volumes of PBS, Dil-labeled ROF NPs and Dil-labeled NE/Dil NPs via the tail vein immediately after MI/R. Images were acquired at 24 h post-MI/R using the *in vivo* IVIS Spectrum Imaging System (PerkinElmer Co. Ltd, MA, USA). Excitation and emission were set at 549 nm and 565 nm, respectively, referring to the instruction of DiI [37]. After *in vitro* imaging, the heart was snap-frozen in liquid nitrogen, and the hearts were embedded in the optimal cutting temperature compound (Tissue-Tek OCT, Sakura Finetek, CA, USA) and serially cut into 5 μm thin sections. Frozen sections were used to observe the fluorescence area of Dil. Image Pro Plus software was used for analysis.

Immunofluorescent staining

Mice were euthanized after 1 day of MI/R and the heart was removed for immunofluorescence. Hearts were made into paraffin sections. The cleavage was washed with PBS for 10 min and then blocked with a blocking solution for 1 h at room temperature. Then, sections were incubated with primary antibodies (ICAM-1, VCAM-1, Ly6G) overnight at 4°C. Next, fluorescent secondary antibodies were incubated with the sections for 2 h at room temperature. Finally, the nuclei were counterstained with DAPI for 5 min and placed under coverslips. Images were taken using a confocal microscope. The results were analyzed with Image Pro Plus software.

Flow cytometry analysis

Neutrophil counts in the peripheral blood of mice were measured by flow cytometry at 24 h after MI/R. Briefly, fresh blood from mice was collected directly through the ophthalmic vein into microcentrifuge tubes containing EDTA (5 mM) using heparin-coated capillaries and immediately placed on ice. Erythrocytes were lysed using BD PharmLyse (BD Biosciences, CA, USA), washed, rinsed and resuspended in fluorescence-activated cell sorter (FACS) buffer (Hanks' balanced salt solution + 0.1% bovine serum albumin w/v, 5 mM EDTA). The cells were stained with an antibody mixture (CD11b-APC monoclonal antibody and Ly6G-PE monoclonal antibody, both Invitrogen [CA, USA]) and incubated in the dark for 30 min on ice. Then, 100 μl of fluorescence-activated cell sorter buffer was added to each sample, filtered through a 74 μm nylon membrane and analyzed by flow cytometry at a constant flow rate and fixed acquisition time.

Evans blue–2,3,5-triphenyl tetrazolium chloride staining

In the next step, 3 days after the MI/R injury, the LAD was relocated with 7-0 sutures, and the aortic root was relocated with 4-0 sutures at the original ligation site through a layer-by-layer thoracotomy under 5% isoflurane anesthesia. Then, 1% Evans blue solution was slowly injected into the left ventricle until the area above the LAD was rapidly blue. Then the hearts were removed and washed with PBS. The hearts were placed in a mold. The plates were incubated in 1.5% 2,3,5-triphenyl tetrazolium chloride (TTC) solution for 30 min at 37°C without light, then removed and photographed. The area of MI was analyzed by Image Pro Plus software: the blue-stained area was viable myocardium, the part not covered by blue dye was ischemic myocardium, the brick-red area was the myocardium saved by reperfusion in the ischemic area and the white area was completely necrotic myocardium. The extent of MI was analyzed using the Image Pro Plus software. After opening the image, the total myocardial area (TA), MI area (brick red + white area, area at risk [AAR]) and myocardial infarction area (IA; white area) were manually recorded. The TA, AAR and IA measured on the positive and negative sides of the same myocardium were averaged, and the total TA (TTA), AAR and total IA (TIA) were calculated by summing the TA, AAR and IA measured on all myocardial sections of the same mouse, respectively. The formula is: AAR% = total AAR/TIA; infract% = TIA/total AAR.

Echocardiography

The cardiac function of the mice was detected on 3 days after MI/R by Visual Sonics Vevo 2100 (Visual-Sonics, Toronto, Canada) small animal high-frequency color ultrasound. After the mice were anesthetized with isoflurane, the left ventricle long axis and short axis sections of the mice were taken, and the left ventricular end-systolic diameter and left ventricular end-diastolic diameter. Left ventricular ejection fraction (LVEF) and left ventricular partial shortening (LVFS) were calculated using the biplane Simpson method and the corresponding software.

Hematoxylin & eosin staining

After cardiac function assessment, mice were sacrificed for histological observation at 7 days post-MI/R. Briefly, the left ventricular myocardium was fixed in 4% paraformaldehyde, transacted, embedded in paraffin, sectioned into 5 μm sections, stained with hematoxylin and eosin (H&E) and examined for morphology. The number of inflammatory cell nuclei was counted by Image Pro Plus software.

Clinical chemistry test

Peripheral blood from mice was collected in eppendorf micro test tubes by enucleation of the eyeball at 7 days after MI/R. The blood was centrifuged at 3000 r.p.m. for 10 min to collect the serum. The plasma concentrations of alanine aminotransferase, aspartate aminotransferase, blood urea nitrogen and creatinine were then quantified using an automated analyzer platform.

Statistical analysis

Statistical analysis was performed using GraphPad Prism (version 9.0). One-way analysis of variance was used for data analysis. The significance level was set to not significant; *$p \leq 0.05$; **$p \leq 0.01$; ***$p \leq 0.001$; ****$p \leq 0.0001$. p-value < 0.05 was considered statistically significant.

Results

Preparation & characterization of neutrophil and endothelial cell membranes coassembled roflumilast NPs

As previously mentioned, neutrophil infiltration and adhesion to ECs play a crucial role in initiating inflammation in MI/R injury [5,43–45]. Based on this rationale, we designed NPs that incorporate fusion membranes of neutrophils and ECs, coated with the PDE4B inhibitor ROF (NE/ROF NPs). Figure 1 illustrates the design of these NE coassembled ROF NPs for targeted therapy in an MI/R injury mouse model. The construction of NE/ROF NPs involved the following steps: firstly, ROF-loaded PLGA NPs (ROF NPs) were prepared using the nanoprecipitation method [38,39]. Next, NE were obtained from their respective 'parent' cells through hypotonic lysis. These membranes were then mixed using the extrusion method, as previously described [37]. Subsequently, the fused cell membranes were coated onto the surface of ROF NPs by sonication and extrusion, facilitating the fusion process [40]. The drug LE of ROF NPs was calculated to be approximately 6.5%, while the EE was determined to be 75%. These results indicated efficient encapsulation of the hydrophobic ROF into the NPs and confirmed that ROF-loaded PLGA NPs are successfully prepared by the nanoprecipitation method. Transmission electron microscope images confirmed the presence of a 'core-shell' structure in the NE/ROF NPs, which was not observed in the ROF NPs (Figure 2A). Additionally, due to the enveloping of the fusion membranes, the size of the NE/ROF NPs increased by approximately 50 nm compared with that of the ROF NPs (Figure 2B). Furthermore, the zeta potential of the NE/ROF NPs was found to be more negative compared with the ROF NPs. This characteristic has been reported to result in longer blood circulation times when compared with NPs with neutral or positive surface charges (Figure 2C) [36,37].

We used dye pairs with FRET properties to label the neutrophil membranes with DiO and Dil, which were then fused with unlabeled EC membranes. Upon the introduction of EC membranes, the fluorescence intensity at 565 nm (Dil) exhibited a decrease (Figure 2D), signifying fusion between the [NE] and attenuation of the fluorescence signal from the acceptor dye Dil [40]. Additionally, we labeled the neutrophil membranes and EC membranes with fluorescent dyes DiD and DiO, respectively, while PLGA was labeled with Dil. CLSM revealed that a majority of the [NE] underwent fusion and encapsulated PLGA (Figure 2E).

To determine whether the proteins on the [NE] had been successfully translocated to the surface of [NE]/NPs, protein analysis was conducted using Coomassie blue staining. The results indicated that [NE]/NPs had similar total protein profiles to those of neutrophil and ECs, suggesting that a majority of the proteins from the [NE] were indeed translocated to the surface of [NE]/NPs (Figure 2F). WB analysis further confirmed the presence of ICAM-1 and VCAM-1 protein signals, indicating the retention of these EC adhesion molecules on [NE]/NPs after membrane coating but not on NPs (Figure 2G). The release kinetics of ROF from ROF NPs and [NE]/ROF NPs were then investigated in buffer solutions simulating the extracellular environment (PBS, pH 7.4) [36]. After 72 h of incubation, 53.33 and 50.33% of ROF were released from ROF NPs and [NE]/ROF NPs, respectively. [NE]/ROF NPs exhibited a slightly slower ROF release profile compared with ROF NPs (Figure 2H). Overall, the steady and prolonged ROF release behavior of [NE]/ROF NPs suggests their potential for sustained drug release.

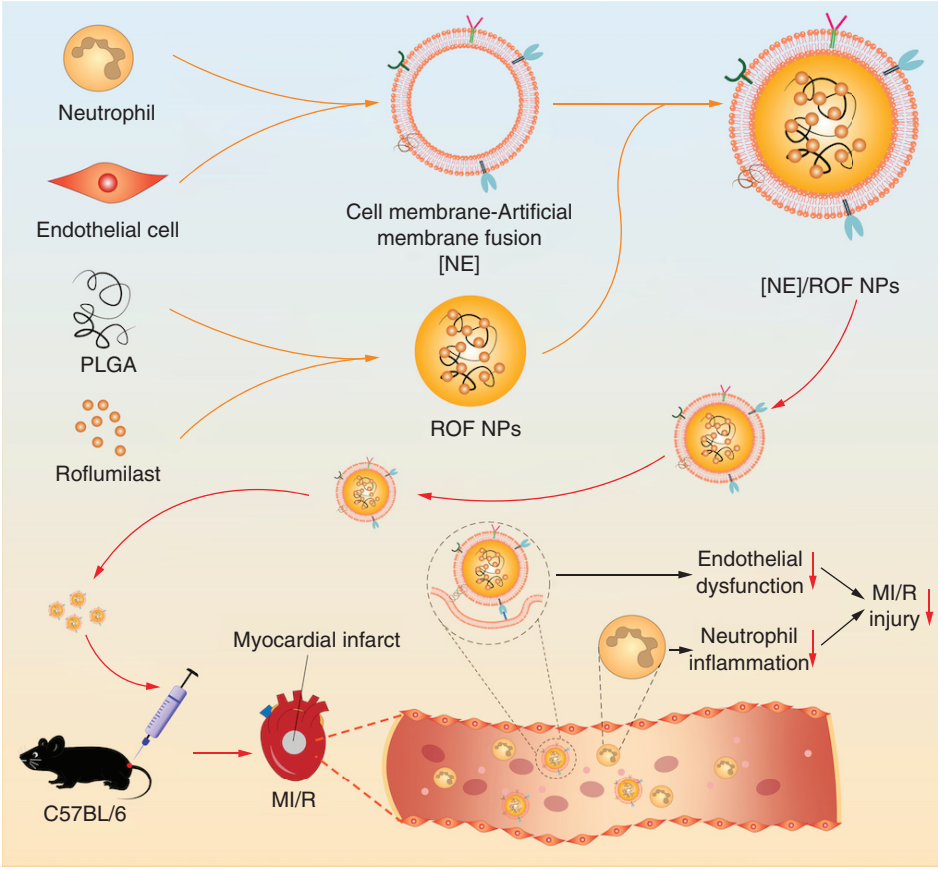

Figure 1. Roflumilast nanoparticles in neutrophil and endothelial cell membranes for the treatment of myocardial ischemia/reperfusion injury.
MI/R: Myocardial ischemia/reperfusion; NE: Neutrophil and endothelial cell membrane; NP: Nanoparticle; PLGA: Poly(lactic-co-glycolic acid); ROF: Roflumilast.

In conclusion, we successfully fused neutrophil membranes with EC membranes and ROF NPs, resulting in the retention of key functional proteins on the [NE]. Importantly, [NE]/ROF NPs were successfully constructed and have the capacity for release.

Evaluation of targeting capacity & efficacy of [NE]/ROF NPs *in vitro*

To assess the targeting effect of [NE]/ROF NPs on activated ECs, we stimulated MAECs with TNF-α, which can simulate activated ECs in the infarcted area after MI/R injury. Afterward, MAECs and activated MAECs were incubated with equal concentrations of DiI NPs and [NE]/DiI NPs for 2 h, and the internalization of NPs was observed. CLSM images showed that [NE]/Dil NPs exhibited higher internalization within activated ECs compared with Dil NPs, displaying stronger red fluorescence signals (Figure 3A & B). Overall, the fusion of [NE] membranes on [NE]/ROF NPs enhanced their uptake by activated ECs, indicating that targeted delivery is a promising strategy in MI/R.

To investigate the anti-inflammatory effect of [NE]/ROF NPs *in vitro*, mouse neutrophil cells (MNHCs) were cultured with LPS for 4 h to simulate the inflammatory environment *in vivo*. Subsequently, the cells were treated with free ROF, ROF NPs or [NE]/ROF NPs for 12 h. The expression of inflammatory factors in MNHCs was determined using quantitative real-time PCR. The results demonstrated an increase in proinflammatory factors such as IL-6 and IL-1β, and a decrease in anti-inflammatory factors such as TGF-β and IL-10 after LPS stimulation. Compared with ROF and ROF NPs, [NE]/ROF NPs significantly reduced the expression of proinflammatory factors and increased the expression of anti-inflammatory factors (Figure 3C–F). Furthermore, the effect of [NE]/ROF NPs on EC adhesion molecules was evaluated. Similarly, MAECs were stimulated with LPS *in vitro* to mimic the inflammatory environment *in vivo* and then cocultured with different forms of ROF for

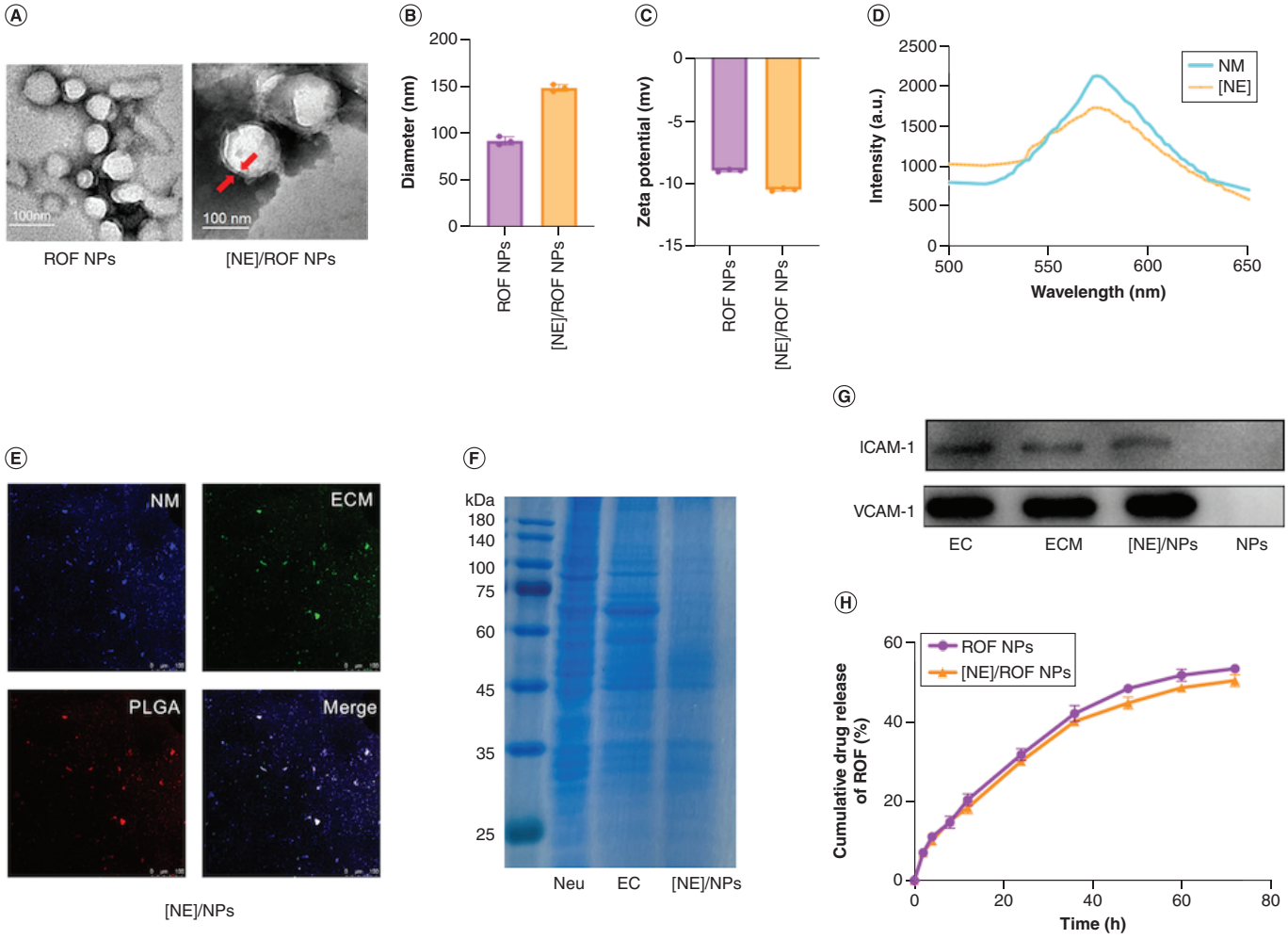

Figure 2. Characterization of roflumilast nanoparticles in neutrophil and endothelial cell membranes. (A) Transmission electron microscope (TEM) image of ROF NPs and [NE]/ROF NPs (scale bar = 100 nm). **(B)** Diameter and **(C)** zeta potential of ROF NPs and [NE]/ROF NPs (n = 3, mean ± SD). **(D)** NMs were labeled with a FRET dye pair DiO and DiI and then fused with endothelial cell membranes. The fluorescence intensity was recorded. **(E)** CLSM images of [NE]/NPs. NM was labeled with DiD (blue), ECM was labeled with DiO (green) and PLGA was labeled with DiI (red) (scale bar = 100 μm). **(F)** Total protein content visualization of Neu, EC and [NE]/NPs stained with Coomassie brilliant blue. **(G)** Western blot identification of ICAM-1, VCAM-1 in EC, ECMs, [NE]/NPs and NPs. **(H)** *In vitro* cumulative drug-release profiles of ROF NPs and [NE]/ROF NPs (n = 3, mean ± SD).
CLSM: Confocal laser scanning microscope; DiD: 1,1′-dioctadecyl-3,3,3′,3′-tetramethylindocarbocyanine, 4-chlorobenzene sulfonate salt; DiI: 1,1′-Dioctadecyl-3,3,3′,3′-tetramethylindocarbocyanineperchlorate; DiO: 3,3′-Dioctadecyloxacarbocyanine perchlorate; EC: Endothelial cell; ECM: Endothelial cell membrane; FRET: Förster resonance energy transfer; NE: Neutrophil and endothelial cell membrane; Neu: Neutrophil; NM: Neutrophil membrane; NP: Nanoparticle; PLGA: Poly(lactic-co-glycolic acid); ROF: Roflumilast; SD: Standard deviation.

12 h. It was found that [NE]/ROF NPs inhibited ICAM-1 expression to a greater extent than free ROF and ROF NPs (Figure 3G–I). Overall, [NE]/ROF NPs demonstrated effective inhibition of neutrophil inflammation and EC adhesion.

Targeting capacity of neutrophil membrane/DiI NPs *in vivo*

Our *in vitro* findings supported the targeting capacity of [NE]/ROF NPs toward inflammatory ECs, indicating their potential for attenuating MI/R injury by suppressing neutrophil inflammation and EC adhesion. To validate these effects *in vivo*, an MI/R mouse model was established. The experimental setup is shown in Figure 4A. Mice underwent LAD ligation for 45 min followed by reperfusion. Immediately after reperfusion, PBS, DiI-labeled ROF NPs or DiI-labeled [NE]/ROF NPs were injected through the caudal vein, with a total volume of 100 μl. Fluorescence intensity in the mice was observed using the IVIS system 24 h after MI/R. The fluorescent intensity of [NE]/ROF NPs in the heart was significantly higher than that of ROF NPs therapy (Figure 4B & C), benefitting

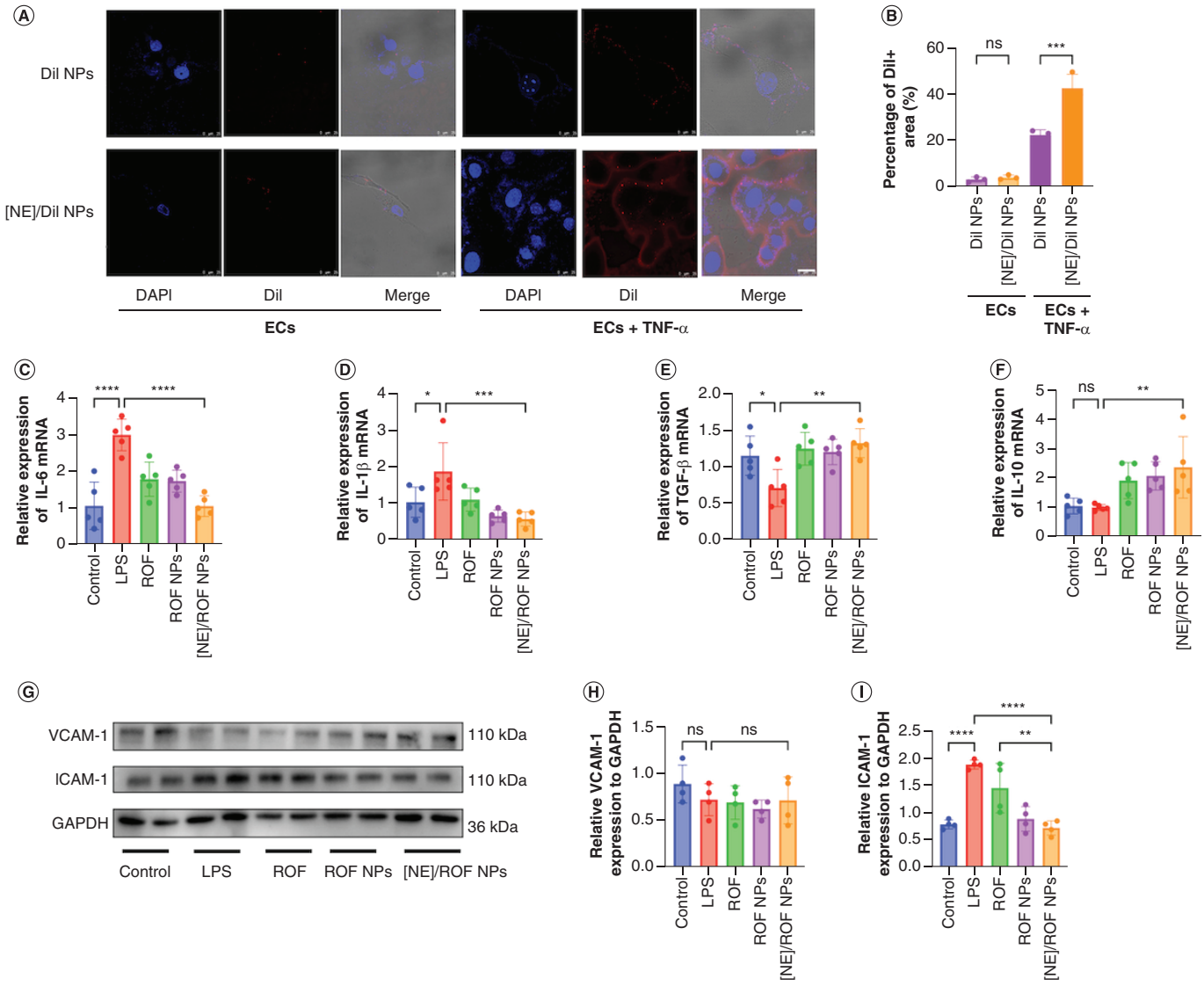

Figure 3. Targeting capacity and anti-inflammation effects of roflumilast nanoparticles in neutrophil and endothelial cell membranes *in vitro*. (A) Representative confocal laser scanning microscope images of cell uptake of Dil NPs, [NE]/Dil NPs after incubation with ECs and activated ECs (stimulated with TNF-α) for 4 h. The nuclei of ECs were stained with DAPI (scale bar = 25 μm). **(B)** Percentage of areas positive for Dil in the field (n = 3, mean ± SD). **(C–F)** Relation expression of inflammatory factor (IL-6, IL-1β, TGF-β, IL-10) mRNA in neutrophils with LPS (1 μg/ml) for 6 h (n = 5, mean ± SD). **(G)** Representative images of western blot assay of adhesion-associated proteins (VCAM-1, ICAM-1). **(H & I)** Quantification of VCAM-1 and ICAM-1 expression (n = 4, mean ± SD). Statistical analyses were performed by one-way ANOVA. All data are shown as the means ± SD.
*p ≤ 0.05; **p ≤ 0.01; ***p ≤ 0.001; ****p ≤ 0.0001.
ANOVA: Analysis of variance; DAPI: 6-Diamidino-2-phenylindole; Dil: 1,1′-Dioctadecyl-3,3,3′,3′-tetramethylindocarbocyanineperchlorate; EC: Endothelial cell; LPS: Lipopolysaccharide; NE: Neutrophil and endothelial cell membrane; NP: Nanoparticle; ns: Not significant; ROF: Roflumilast: SD: Standard deviation.

from neutrophil chemotactic targeting [33,43,44]. After *in vitro* imaging, frozen sections were used to observe the fluorescence area of Dil in the hearts of mice. [NE]/ROF NPs detected a higher amount of Dil dye in the ischemic site of the heart compared with ROF NPs (Figure 4D & E). The fluorescence intensity in the major organs (hearts, lungs, livers, spleens and kidneys) of mice was visualized and the existence or not of toxicity in the life organism at 7 d after intravenous injection Dil-labeled NPs. The results revealed that [NE]/ROF Dil NPs injection exhibited significant accumulation in the heart at 7 d after injection, which was facilitated by neutrophil chemotaxis targeting. A large number of NPs were also observed to accumulate in the liver and kidney (Figure 4F & G). The results demonstrated that [NE]/ROF NPs exhibited the highest accumulation in the injured heart in MI/R mice.

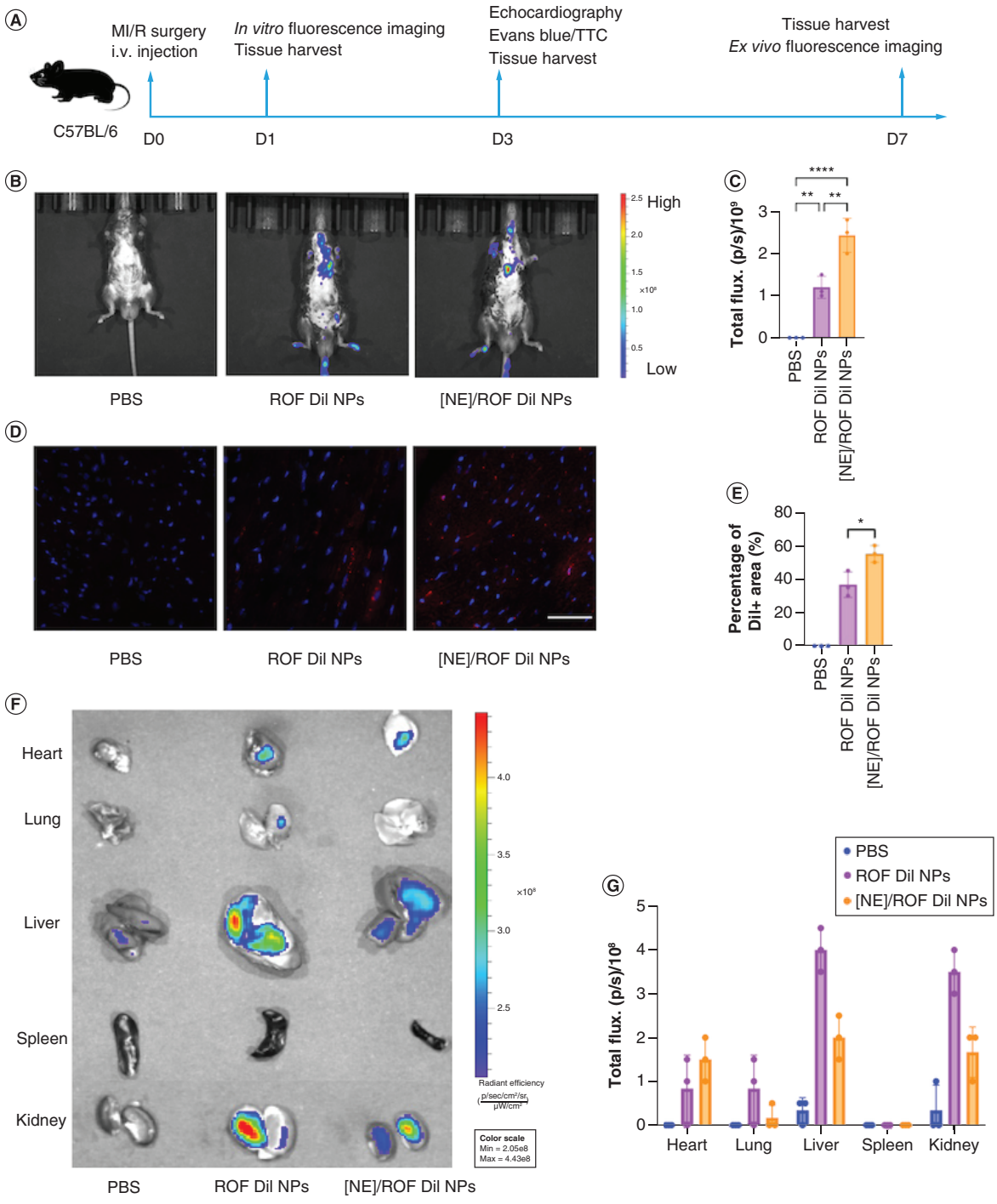

Figure 4. ***In vivo*** **targeting capacity of roflumilast nanoparticles in neutrophil and endothelial cell membranes in mice model of myocardial ischemia/reperfusion. (A)** Experiment setup in this study. **(B)** Representative *in vivo* images of mice after intravenous injection of PBS, Dil-ROF NPs and Dil-[NE]/ROF NPs at 24 h post-MI/R. **(C)** Quantifying fluorescent intensity in hearts (n = 3, mean ± SD). **(D)** Representative confocal laser scanning microscope images of Dil fluorescence dye in the hearts at 24 h postintravenous injection of Dil-labeled NPs (scale bar = 50 μm). **(E)** Percentage of areas positive for DiI in the visual field (n = 3, mean ± SD). **(F)** *Ex vivo* fluorescent images of major organs at 7 days after intravenous injection Dil-labeled NPs. **(G)** Quantification of fluorescent intensity in major organs (n = 3, mean ± SD). All data are shown as the means ± SD. Statistical analyses were performed by one-way ANOVA. *p ≤ 0.05; **p ≤ 0.01; ****p ≤ 0.0001.

ANOVA: Analysis of variance; Dil: 1,1′-Dioctadecyl-3,3,3′,3′-tetramethylindocarbocyanineperchlorate; MI/R: Myocardial ischemia/reperfusion; NE: Neutrophil and endothelial cell membrane; NP: Nanoparticle; PBS: Phosphate-buffer solution; ROF: Roflumilast: SD: Standard deviation.

[NE]/ROF NPs inhibited neutrophil infiltration & EC adhesion molecule expression in the myocardium after myocardial ischemia/reperfusion

The early stage of AMI is the inflammatory stage, during which extensive death of cardiomyocytes occurs, triggering sterile inflammation that recruits and activates a large number of inflammatory cells, primarily neutrophils [46–48]. To determine the effect of [NE]/ROF NPs on myocardial inflammation after MI/R, H&E staining was utilized to observe the infiltration of inflammatory cells in the hearts of the three groups of mice at 3 d after MI/R. The results demonstrated that the number of infiltrating inflammatory cells in the peripheral area of myocardial infarction in the [NE]/ROF NPs group was significantly lower compared with the PBS group, free ROF group and ROF NPs group. This finding suggested that [NE]/ROF NPs efficiently reduced the infiltration of inflammatory cells in the myocardium after reperfusion (Figure 5A & B). Previous studies have shown that neutrophil recruitment increases within 6 h after AMI and peaks at 24 h [49]. The number of neutrophils in the blood follows a similar pattern. Therefore, we collected peripheral blood for flow cytometry at 24 h after MI/R and observed an increase in the number of neutrophils after MI/R. [NE]/ROF NPs demonstrated more effective inhibition of elevated neutrophils compared with ROF and ROF NPs (Figure 5C & D). Immunofluorescence staining of the heart yielded similar results (Figure 5E), suggesting that [NE]/ROF NPs had a greater ability to inhibit neutrophil inflammatory response and infiltration in the infarcted area.

We then investigated the effects of [NE]/ROF NPs on neutrophil–endothelial interactions, which represent an early stage in neutrophil recruitment. We examined the expression of adhesion molecules in the ischemic area of MI/R-injured hearts. Immunofluorescence and WB results revealed that treatment with [NE]/ROF NPs significantly reduced the expression of VCAM-1 and ICAM-1 compared with treatment with ROF and ROF NPs (Figure 6A–D). Furthermore, we confirmed that [NE]/ROF NPs, ROF and ROF NPs all decreased PDE4B expression, but there was no significant difference between the groups (Figure 6E). These findings suggested that [NE]/ROF NPs offered protection against MI/R injury by enhancing the effectiveness of ROF, as well as inhibiting neutrophil infiltration and EC adhesion.

[NE]/ROF NPs attenuated MI/R injury

Previous research has shown that ROF, a PDE4 inhibitor, improves cardiac microcirculation, suppresses inflammation and attenuates MI/R injury in mice [5,15]. To investigate the potential of [NE]/ROF NPs in attenuating MI/R injury, we utilized Evans blue/TTC staining to assess MI/R injury at 3 d postreperfusion (Figure 7A). [NE]/ROF NPs-treated mice exhibited significantly smaller infarct sizes compared with those treated with ROF and ROF NPs, despite similar regions at risk (AAR) (Figure 7B & C), suggesting that [NE]/ROF NPs possess greater potential in improving cardiac function following MI/R injury.

Echocardiography was conducted at 3 d post-MI/R surgery to assess cardiac function (Figure 7D). As expected, the data revealed a significant decrease in LVEF (LVEF%) and fractional shortening of the short axis (LVFS%) in the PBS group. Interestingly, both ROF NPs and [NE]/ROF NPs groups exhibited a significant increase in LVEF% and LVFS% compared with the ROF group, with the [NE]/ROF NPs group displaying a stronger effect than the ROF NPs group (Figure 7E & F). Notably, there were no significant differences observed in left ventricular end-diastolic diameter and left ventricular end-systolic diameter among the groups (Figure 7G & H). These results suggest that [NE]/ROF NPs possessed an enhanced ability to preserve cardiac function, likely due to their biomimetic fusion membrane structure.

Biosafety of [NE]/ROF NPs *in vivo*

During drug therapy, NPs-associated toxic side effects on normal organs and the overall system have been a significant concern [50]. Therefore, to evaluate the biosafety of [NE]/ROF NPs, any potential side effects were investigated after 7 d of treatment. The H&E staining results revealed no noticeable changes or damage to major organs in the PBS, ROF, ROF NPs and [NE]/ROF NPs groups, indicating minimal safety concerns associated with these NPs (Figure 8A). Additionally, clinical biochemical analysis demonstrated that serum levels of alanine aminotransferase, aspartate aminotransferase, urea nitrogen and creatinine remained within the normal range between PBS, ROF, ROF NPs and [NE]/ROF NPs groups, indicating that the treatment did not adversely affect liver and kidney functions, thus confirming their biocompatibility (Figure 8B–E).

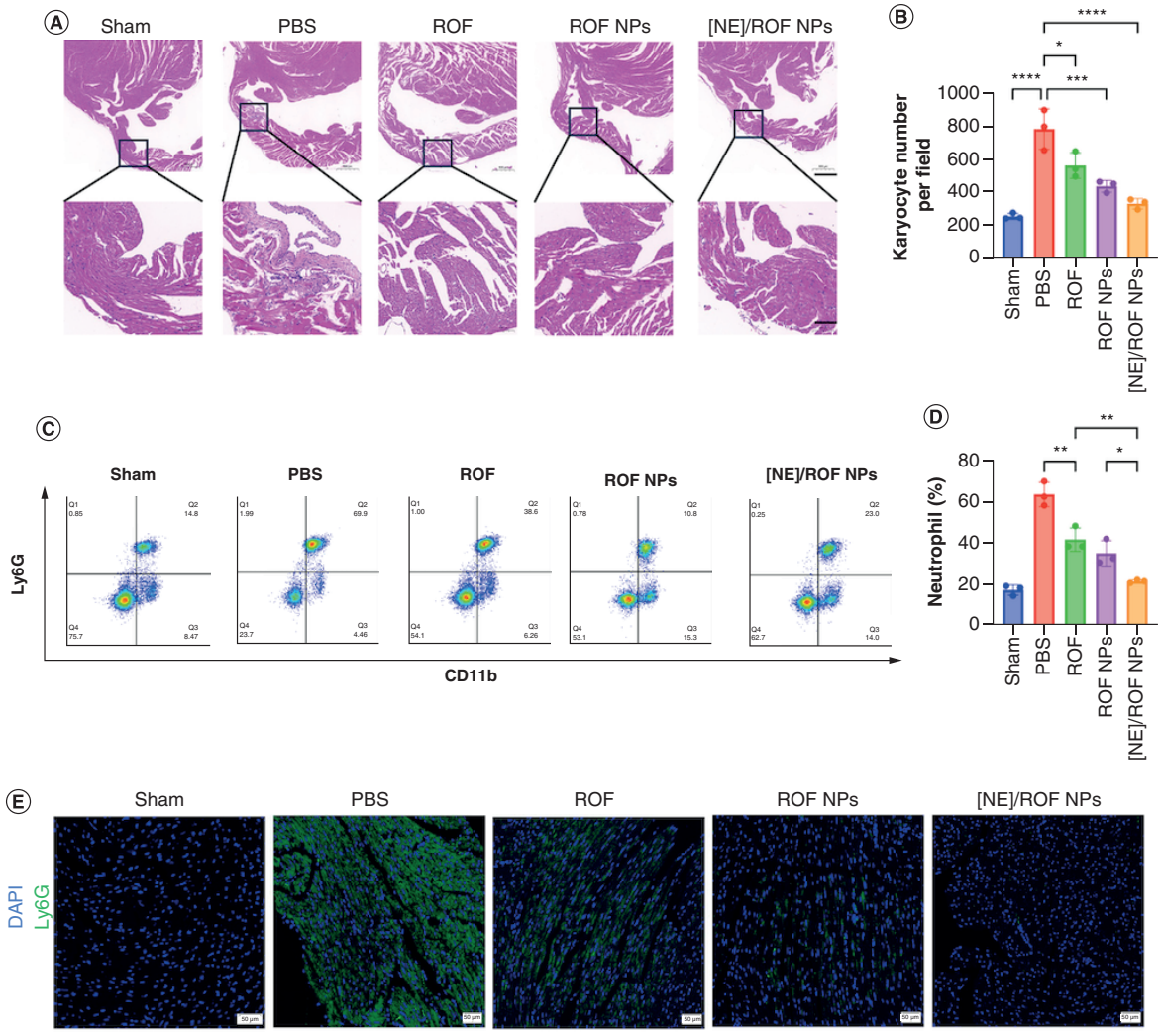

Figure 5. Roflumilast nanoparticles in neutrophil and endothelial cell membranes reduced neutrophil infiltration in the myocardium after myocardial ischemia/reperfusion. (A) Representative images of H&E staining at 3 d after MI/R surgery (scale bar = 500 μm [upper] and 100 μm [lower]). **(B)** Percentage of inflammatory cells in the peri-infarct zone (n = 3, mean ± SD). **(C)** Representative flow cytometry plots of neutrophil (CD11b+Ly6G+) population in the peripheral blood of mice at 1 d after MI/R surgery. **(D)** Quantification of neutrophil in peripheral blood 1 d following treatment (n = 3, mean ± SD). **(E)** Representative fluorescent images of Ly6G (green) in frozen sections of infarcted area in heart; nuclei were stained with DAPI (blue) (scale bar = 50 μm). All data are shown as the means ± SD. Statistical analyses were performed by one-way ANOVA.
*p ≤ 0.05; ***p ≤ 0.001; ****p ≤ 0.0001.
ANOVA: Analysis of variance; d: Day; DAPI: 6-Diamidino-2-phenylindole; H&E: Hematoxylin and eosin; MI/R: Myocardial ischemia/reperfusion; NE: Neutrophil and endothelial cell membrane; NP: Nanoparticle; ROF: Roflumilast; SD: Standard deviation.

Discussion

MI/R injury is an inevitable pathological process that occurs after revascularization of AMI. This process can lead to microcirculation disturbance in myocardial tissue, oxidative stress-induced cell damage, notable inflammatory response and further myocardial cell necrosis [7]. Therefore, active and effective inhibition of MI/R injury after blood flow restoration in patients with AMI holds significant importance for preserving damaged cardiac muscle and improving patient prognosis. We developed [NE] coassembled ROF NPs to attenuate MI/R injury in our study. This approach will help salvage damaged cardiac muscle and improve the prognosis of patients.

In patients with AMI, neutrophil counts have been identified as an independent prognostic factor after percutaneous coronary intervention. The level of neutrophils in the bloodstream is directly correlated with the infarct size

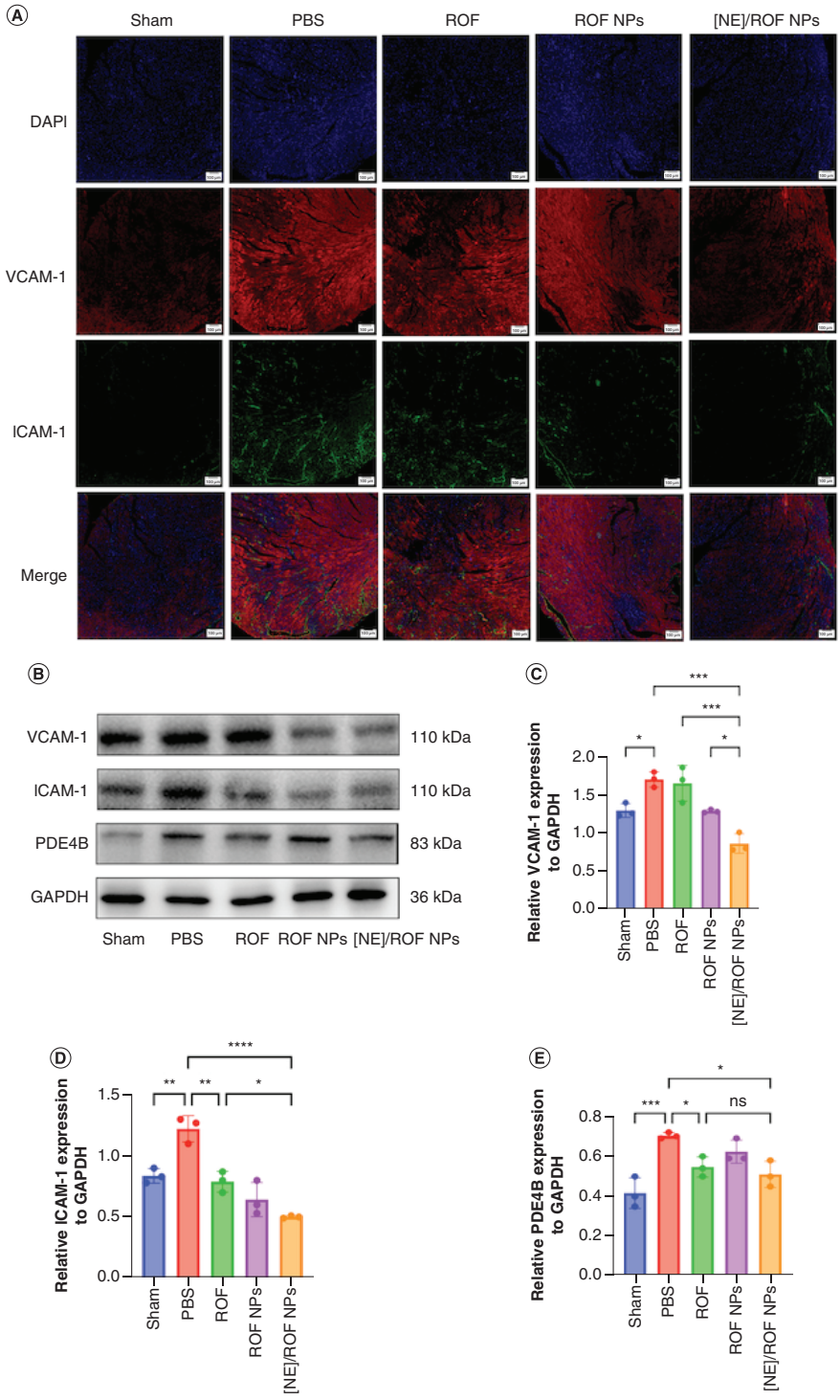

Figure 6. Roflumilast nanoparticles in neutrophil and endothelial cell membranes suppressed endothelial cell adhesion molecule expression in the myocardium after myocardial ischemia/reperfusion. (A) Representative images of VCAM-1 (red) and ICAM-1 (green) on the heart sections, and nuclei were stained with DAPI (blue) (scale bar = 100 μm). **(B)** Representative images of western blot assay of VCAM-1, ICAM-1 and PDE4B. **(C–E)** Quantification of VCAM-1, ICAM-1 and PDE4B expression (n = 3, mean ± SD). All data are shown as the means ± SD. Statistical analyses were performed by one-way ANOVA.
*$p \leq 0.05$; **$p \leq 0.01$; ***$p \leq 0.001$; ****$p \leq 0.0001$.
ANOVA: Analysis of variance; DAPI: 6-Diamidino-2-phenylindole; MI/R: Myocardial ischemia/reperfusion; NE: Neutrophil and endothelial cell membrane; NP: Nanoparticle; ns: Not significant; ROF: Roflumilast; SD: Standard deviation.

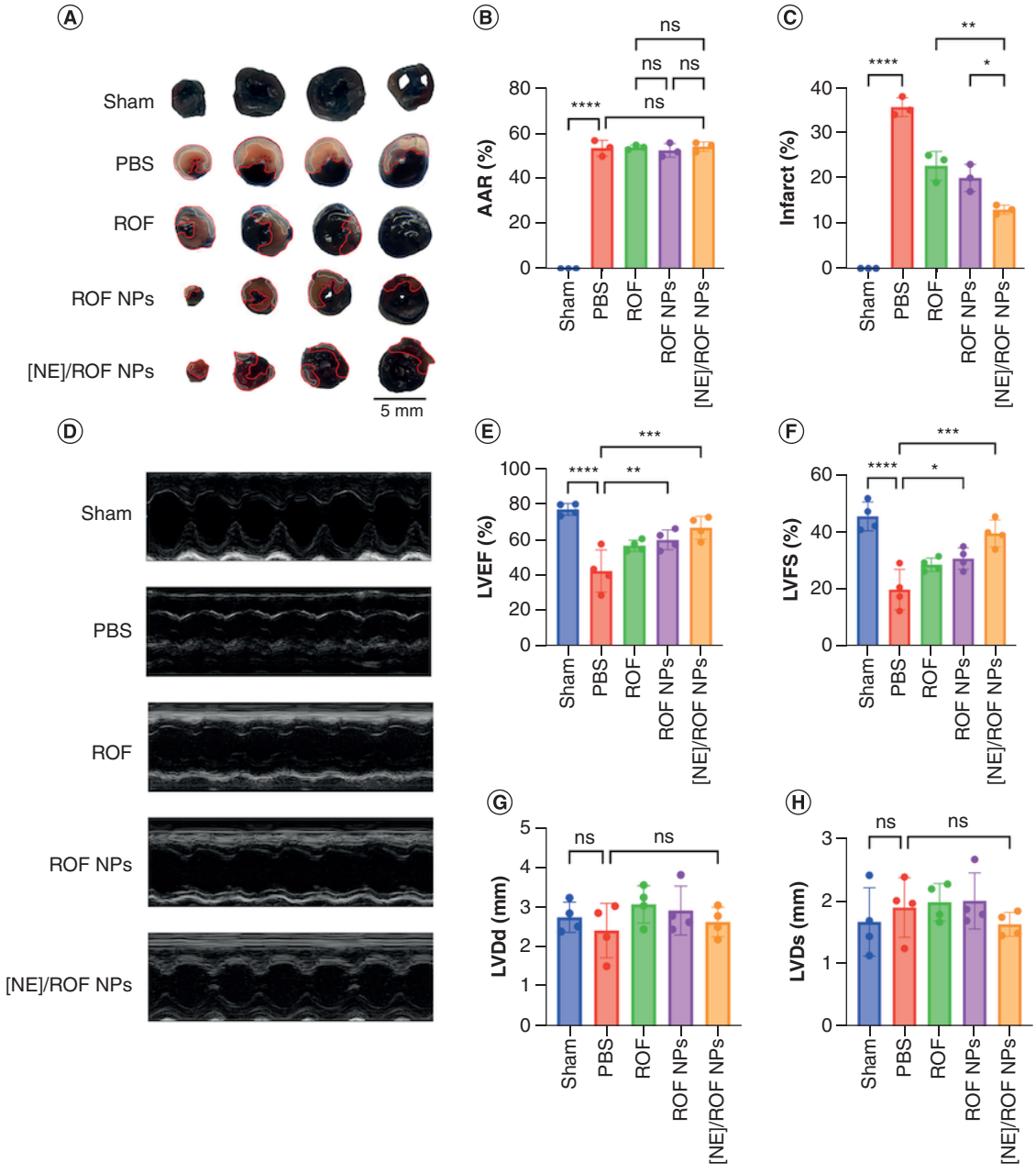

Figure 7. Roflumilast nanoparticles in neutrophil and endothelial cell membranes nanoparticles attenuated myocardial ischemia/reperfusion injury. (A) Representative images of Evans blue and TTC-stained hearts from mice at 3 d after MI/R. AAR (red line) and IS (white dotted line) (scale bar = 5 mm). **(B & C)** Quantification of percentage AAR and percentage infarct in hearts (n = 3). **(D)** Representative echocardiographic images of mice at 3 d post-MI/R. **(E–H)** Quantification of LVEF%, LVFS%, LVDd and LVDs (n = 4, mean ± SD). All data are shown as the means ± SD. Statistical analyses were performed by one-way ANOVA.
*p ≤ 0.05; **p ≤ 0.01; ***p ≤ 0.001; ****p ≤ 0.0001.
AAR: Area at risk; ANOVA: Analysis of variance; d: Day; IS: Infarct size; LVDd: Left ventricular end-diastolic diameter; LVDs: Left ventricular end-systolic diameter; LVEF: Left ventricular ejection fraction; LVFS: Left ventricular partial shortening; MI/R: Myocardial ischemia/reperfusion; NE: Neutrophil and endothelial cell membrane; NP: Nanoparticle; ns: Not significant; ROF: Roflumilast; SD: Standard deviation; TTC: 2,3,5-triphenyl tetrazolium chloride.

Taylor & Francis
Taylor & Francis Group

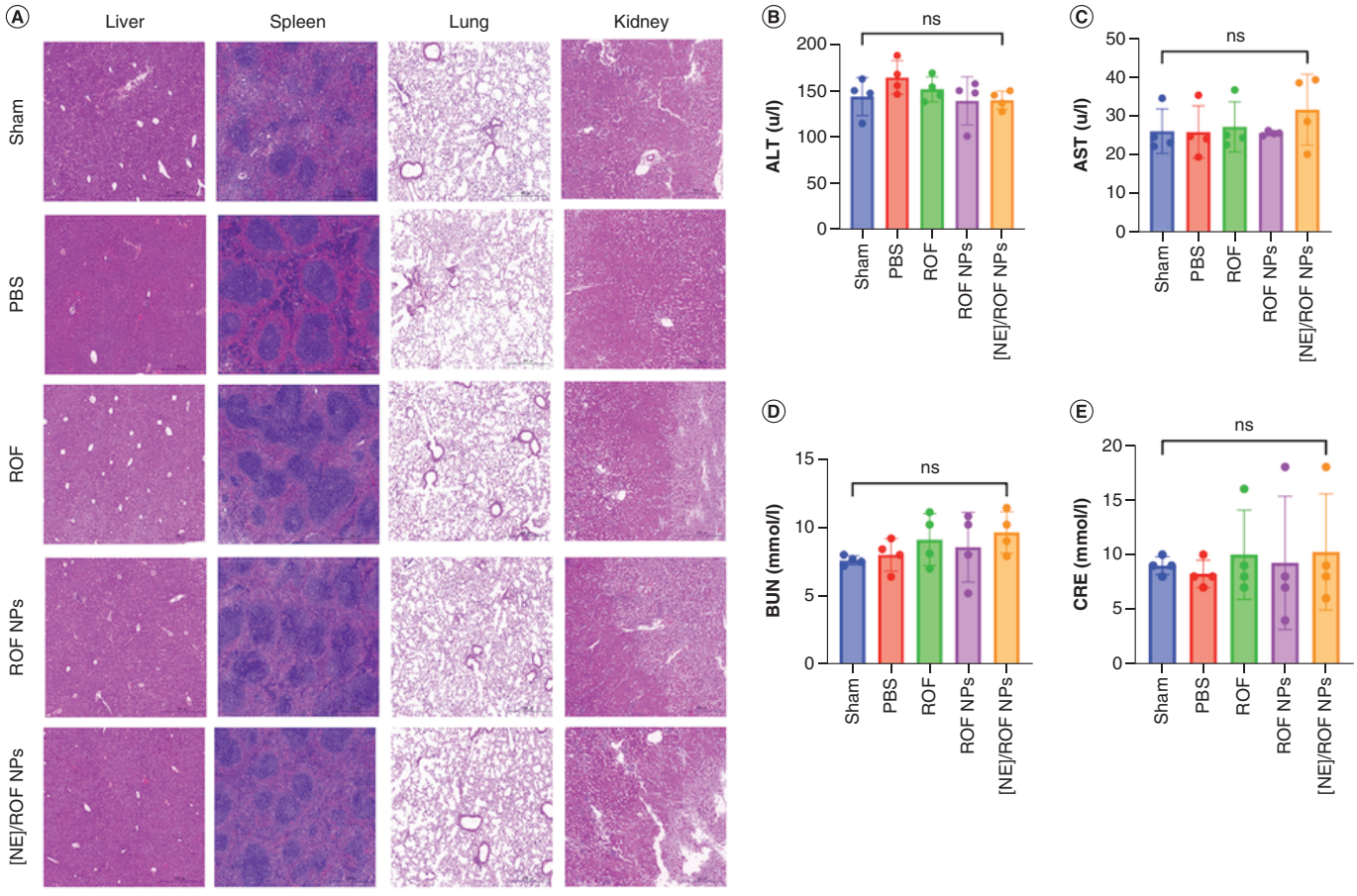

Figure 8. Safety evaluation of roflumilast nanoparticles in neutrophil and endothelial cell membranes. (A) H&E staining of histological sections from major organs (liver, spleen, lung, kidney) 7 d after injection (scale bar = 500 μm). **(B–E)** Biochemical markers relevant to hepatic and kidney function (n = 4, mean ± SD).
d: Day; H&E: Hematoxylin and eosin; NE: Neutrophil and endothelial cell membrane; NP: Nanoparticle; ns: Not significant; ROF: Roflumilast; SD: Standard deviation.

and LVEF% [49]. Furthermore, ECs play a crucial role in vascular anti-inflammatory processes [51]. ICAM-1 and VCAM-1, which are intercellular adhesion molecules on ECs, bind to neutrophils and facilitate their adhesion, rolling and infiltration [52]. Our study has demonstrated that expression of VCAM-1 or ICAM-1 was elevated in ECs after inflammatory stimulation and in infarcted hearts after MI/R. Using inflammation as the cue, drug or treatment systems targeting neutrophils or upregulated markers such as VCAM-1 and ICAM-1 will have a protective effect on AMI and MI/R injury.

In recent years, the development of NPs has expanded into a broad range of clinical applications [22]. PLGA is an ideal material for codelivery of drugs, which can be hydrophobic and hydrophilic compounds, as well as different molecular weights, such as small molecules, biological macromolecules, proteins and vaccines. By adjusting the composition, stability, reactivity and surface charge of NPs and drugs, the loading effect and release kinetics of drugs can be precisely controlled. PLGA is finally degraded into carbon dioxide and water *in vivo*. For these reasons, PLGA is the most common class of US FDA-approved nanomedicines [22]. Once NPs enter the blood circulation, NPs can be distributed and accumulate in different organs such as the heart, liver, lung, kidney and other organs, with eventual clearance of NPs through the liver or kidneys [53]. So, we chose PLGA NPs as a nanodelivery system used in mice in our study with the expectation of its future application in humans.

While NPs can increase drug loading and tissue drug concentration, which has been applied in the process of drug delivery, it has the defects of not targeting and being easily recognized and swallowed by the macrophage system. After entering the body, most of the drugs carried by NPs cannot reach the target organ through the systemic circulation system. Natural cell membrane-coated NPs are becoming a promising drug-delivery strategy due to

their low immunogenicity, long half-life, low toxicity and innate targeting [54]. Commonly used cell membrane sources include red blood cells, neutrophils, tumor cells, platelets, exosomes, stem cells, etc. [35]. Different types of cell membranes have their own special characteristics and can be used for the diagnosis and treatment of different diseases. Neutrophil membrane loaded with antibiotics can actively target to the site of inflammatory injury under the effect of chemotaxis, and play an anti-inflammatory role [55]. EC membrane expresses adhesion molecules ICAM-1 and VCAM-1, which can competitively inhibit the adhesion of neutrophils in the infarct area of the heart after MI/R. Thus, in this research, we fused natural [NE] and developed a hybrid biomimetic NPs system for the MI/R injury treatment.

ROF, a PDE4 inhibitor, blocks the hydrolysis of cAMP via inhibition of PDE4 and is an attractive candidate for novel anti-inflammatory drugs. It was previously reported that high-concentration NO induces apoptosis in H9c2 cells [56]. Kwak *et al.* demonstrated ROF protects cardiomyocytes against NO-induced apoptosis via activation of PKA and Epac dual pathways [14]. Bonato *et al.* found ROF attenuated blood–brain barrier disruption and restored the levels of endothelial NO synthase in the CA1 hippocampal area [57]. However, the therapeutic effect of ROF is hindered by its comparatively narrow therapeutic window and some side effects such as weight loss, headaches, atrial fibrillation and so on. In addition, the administration of ROF needs high frequency and complex time points in MI/R. Therefore, targeted drug-delivery systems are urgently needed to increase the accumulation of ROF in infarct hearts and reduce severe side effects.

Based on the results of previous studies, we hypothesized that [NE]/ROF NPs could restore the levels of endothelial NO synthase in ECs thus attenuating MI/R injury [57,58]. In our study, we only focused on that [NE]/ROF NPs had a greater ability to inhibit neutrophil inflammatory response and infiltration in the infarcted area. *In vivo* and *in vitro* studies demonstrated that [NE]/ROF NPs exhibited significant anti-inflammatory and antiadhesion effects, and they effectively reduced infarct size and improved cardiac function after MI/R. There was no significant change in body weight between ROF, ROF NPs and [NE]/ROF NPs groups at 7 d after MI/R (Supplementary Figure 2). Additionally, our biomimetic targeting system was safe and harmless, with no obvious adverse effects *in vivo*.

There are some limitations in our study. We did not carry out some cytokine assay in blood or tissue samples after the injection of the different NPs. We only focused on inflammatory infiltration and neutrophil count through H&E staining and flow cytometry, respectively. Our study only examined histopathology within 7 d after MI/R surgery of mice. We prefer to extend longer time scales to visualize the existence or toxicity in the life organism after the exposure of [NE]/ROF NPs in our following works. In the following study, we would like to explore the mechanism that [NE]/ROF NPs act on cardiomyocytes and mitochondria in the I/R heart.

Conclusion

In summary, we have developed biocompatible biomimetic bifunctionally targeted NPs, [NE]/ROF NPs, based on the aforementioned characteristics of neutrophils and ECs. These NPs possess the traits inherited from their parent cells and exhibit inflammatory targeting as well as competitive inhibition of adhesion molecule expression at the damaged myocardium site. The [NE]/ROF NPs enhance the anti-inflammatory and antiadhesion abilities of ROF both *in vivo* and *in vitro*, and effectively deliver ROF to the injured myocardium, resulting in improved cardiac function and reduced infarct size following MI/R. This study shed new light on the application of [NE]/ROF NPs as a potential therapeutic agent for MI/R injury. Furthermore, the biomimetic drug-delivery system also can be extended to be applied for the treatment of other inflammatory diseases.

Supplementary data

To view the supplementary data that accompany this paper please visit the journal website at: www.futuremedicine.com/doi/suppl/10.2217/nnm-2023-0313

Financial disclosure

The present study was funded by the National Key Research and Development Plan 14th Five-Year Nano Frontier Key Special Project (2022YFA1205904), the National Natural Science Foundation of China (82100478), the Jiangsu Planned Projects for Postdoctoral Research Funds (2021K287B), the Natural Science Foundation of Jiangsu Province (BK20200128) and the Nanjing Medical Science and Technology Development Project (YKK21070). The authors have no other relevant affiliations or financial involvement with any organization or entity with a financial interest in or financial conflict with the subject matter or materials discussed in the manuscript apart from those disclosed.

Summary points

- Myocardial ischemia/reperfusion (MI/R) injury is an unavoidable consequence of revascularization in patients with acute myocardial infarction.
- Neutrophils and endothelial cells are pivotal in MI/R injury's pathophysiology.
- Phosphodiesterase 4B is critically involved in neutrophil inflammation and microvascular obstruction, leading to MI/R injury.
- We successfully synthesized neutrophil and endothelial cell membrane ([NE])/roflumilast (ROF) nanoparticles (NPs) by assembling ROF NPs in [NE].
- [NE]/ROF NPs exhibited significant anti-inflammatory and antiadhesion effects, and they could inhibit neutrophil infiltration and endothelial cell adhesion after MI/R.
- Administration of [NE]/ROF NPs after reperfusion was more effective than ROF and ROF NPs alone in improving cardiac function, inhibiting inflammation and reducing MI/R injury in mice.
- [NE]/ROF NPs exhibited stronger targeting capabilities and demonstrated good safety profiles compared with other treatments.
- These findings highlight the potential of [NE]/ROF NPs as a versatile biomimetic drug-delivery system for effectively addressing MI/R injury.

Competing interests disclosure

The authors have no competing interests or relevant affiliations with any organization or entity with the subject matter or materials discussed in the manuscript. This includes employment, consultancies, honoraria, stock ownership or options, expert testimony, grants or patents received or pending, or royalties.

Writing disclosure

No writing assistance was utilized in the production of this manuscript.

Ethical conduct of research

All animal experimental procedures were approved by the Institutional Ethics Committee of Nanjing Drum Tower Hospital (approval no. 2021AE02005).

Data availability statement

The data that support the findings of this study are available from the corresponding author upon reasonable request.

References

Papers of special note have been highlighted as: • of interest; •• of considerable interest

1. Reed GW, Rossi JE, Cannon CP. Acute myocardial infarction. *Lancet* 389(10065), 197–210 (2017).
2. Yeh RW, Sidney S, Chandra M, Sorel M, Selby JV, Go AS. Population trends in the incidence and outcomes of acute myocardial infarction. *N. Engl. J. Med.* 362(23), 2155–2165 (2010).
3. Salari N, Morddarvanjoghi F, Abdolmaleki A *et al.* The global prevalence of myocardial infarction: a systematic review and meta-analysis. *BMC Cardiovasc. Disord.* 23(1), 206 (2023).
4. Dyrbus K, Gasior M, Desperak P, Osadnik T, Nowak J, Banach M. The prevalence and management of familial hypercholesterolemia in patients with acute coronary syndrome in the Polish tertiary centre: results from the TERCET registry with 19,781 individuals. *Atherosclerosis* 288, 33–41 (2019).
5. Wan Q, Xu C, Zhu L *et al.* Targeting PDE4B (phosphodiesterase-4 subtype B) for cardioprotection in acute myocardial infarction via neutrophils and microcirculation. *Circ. Res.* 131(5), 442–455 (2022).

•• **The innovation of our study referred to the mechanism of this article: phosphodiesterase 4B deficiency or pharmacological inhibition reduced coronary microvascular obstruction and infarct size and protected heart function after myocardial ischemia/reperfusion injury.**

6. Davidson SM, Ferdinandy P, Andreadou I *et al.* Multitarget strategies to reduce myocardial ischemia/reperfusion injury: JACC review topic of the week. *J. Am. Coll. Cardiol.* 73(1), 89–99 (2019).
7. Heusch G. Myocardial ischaemia–reperfusion injury and cardioprotection in perspective. *Nat. Rev. Cardiol.* 17(12), 773–789 (2020).

8. Deftereos S, Giannopoulos G, Angelidis C *et al.* Anti-inflammatory treatment with colchicine in acute myocardial infarction: a pilot study. *Circulation* 132(15), 1395–1403 (2015).
9. Garcia-Prieto J, Villena-Gutierrez R, Gomez M *et al.* Neutrophil stunning by metoprolol reduces infarct size. *Nat. Commun.* 8, 14780 (2017).
10. Kolb M, Crestani B, Maher TM. Phosphodiesterase 4B inhibition: a potential novel strategy for treating pulmonary fibrosis. *Eur. Respir. Rev.* 32(167), (2023).
11. Halpin DMG, Criner GJ, Papi A *et al.* Global initiative for the diagnosis, management, and prevention of chronic obstructive lung disease. The 2020 GOLD Science Committee report on COVID-19 and chronic obstructive pulmonary disease. *Am. J. Respir. Crit. Care Med.* 203(1), 24–36 (2021).
12. Rabe KF. Update on roflumilast, a phosphodiesterase 4 inhibitor for the treatment of chronic obstructive pulmonary disease. *Br. J. Pharmacol.* 163(1), 53–67 (2011).
13. Xu B, Xu J, Cai N *et al.* Roflumilast prevents ischemic stroke-induced neuronal damage by restricting GSK3beta-mediated oxidative stress and IRE1alpha/TRAF2/JNK pathway. *Free Radic. Biol. Med.* 163, 281–296 (2021).
14. Kwak HJ, Park KM, Choi HE, Chung KS, Lim HJ, Park HY. PDE4 inhibitor, roflumilast protects cardiomyocytes against NO-induced apoptosis via activation of PKA and Epac dual pathways. *Cell. Signal.* 20(5), 803–814 (2008).
15. Liao B, Han Z. Roflumilast reduces myocardial ischemia reperfusion injury *in vivo* and *in vitro* by activating the AMPK signaling pathway. *Exp. Ther. Med.* 25(6), 302 (2023).
16. Bhat A, Ray B, Mahalakshmi AM *et al.* Phosphodiesterase-4 enzyme as a therapeutic target in neurological disorders. *Pharmacol. Res.* 160, 105078 (2020).
17. Kim M, Lee JH, Nam JM. Plasmonic photothermal nanoparticles for biomedical applications. *Adv. Sci. (Weinh.)* 6(17), 1900471 (2019).
18. Feng X, Xu W, Li Z, Song W, Ding J, Chen X. Immunomodulatory nanosystems. *Adv. Sci. (Weinh.)* 6(17), 1900101 (2019).
19. Wang D, Wang S, Zhou Z *et al.* White blood cell membrane-coated nanoparticles: recent development and medical applications. *Adv. Healthc. Mater.* 11(7), e2101349 (2022).
20. Dash P, Piras AM, Dash M. Cell membrane coated nanocarriers – an efficient biomimetic platform for targeted therapy. *J. Control. Rel.* 327, 546–570 (2020).
21. Zhao L, Seth A, Wibowo N *et al.* Nanoparticle vaccines. *Vaccine* 32(3), 327–337 (2014).
22. Mitchell MJ, Billingsley MM, Haley RM, Wechsler ME, Peppas NA, Langer R. Engineering precision nanoparticles for drug delivery. *Nat. Rev. Drug Discov.* 20(2), 101–124 (2021).
23. Liu Y, Luo J, Chen X, Liu W, Chen T. Cell membrane coating technology: a promising strategy for biomedical applications. *Nanomicro Lett.* 11(1), 100 (2019).
24. Oroojalian F, Beygi M, Baradaran B, Mokhtarzadeh A, Shahbazi MA. Immune cell membrane-coated biomimetic nanoparticles for targeted cancer therapy. *Small* 17(12), e2006484 (2021).
25. Fang RH, Gao W, Zhang L. Targeting drugs to tumours using cell membrane-coated nanoparticles. *Nat. Rev. Clin. Oncol.* 20(1), 33–48 (2023).
26. Jan N, Madni A, Khan S *et al.* Biomimetic cell membrane-coated poly(lactic-co-glycolic acid) nanoparticles for biomedical applications. *Bioeng. Transl. Med.* 8(2), e10441 (2023).
27. Fang RH, Hu CM, Luk BT *et al.* Cancer cell membrane-coated nanoparticles for anticancer vaccination and drug delivery. *Nano Lett.* 14(4), 2181–2188 (2014).
28. Algar WR, Hildebrandt N, Vogel SS, Medintz IL. FRET as a biomolecular research tool – understanding its potential while avoiding pitfalls. *Nat. Methods* 16(9), 815–829 (2019).
29. Stahelin RV. Surface plasmon resonance: a useful technique for cell biologists to characterize biomolecular interactions. *Mol. Biol. Cell* 24(7), 883–886 (2013).
30. Lostao A, Lim K, Pallares MC, Ptak A, Marcuello C. Recent advances in sensing the inter-biomolecular interactions at the nanoscale – a comprehensive review of AFM-based force spectroscopy. *Int. J. Biol. Macromol.* 238, 124089 (2023).
31. Prabhu SD, Frangogiannis NG. The biological basis for cardiac repair after myocardial infarction: from inflammation to fibrosis. *Circ. Res.* 119(1), 91–112 (2016).
32. Kelly M, Hwang JM, Kubes P. Modulating leukocyte recruitment in inflammation. *J. Allergy Clin. Immunol.* 120(1), 3–10 (2007).
33. Han D, Wang F, Qiao Z *et al.* Neutrophil membrane-camouflaged nanoparticles alleviate inflammation and promote angiogenesis in ischemic myocardial injury. *Bioact. Mater.* 23, 369–382 (2023).
34. Visweswaran GR, Gholizadeh S, Ruiters MH, Molema G, Kok RJ, Kamps JA. Targeting rapamycin to podocytes using a vascular cell adhesion molecule-1 (VCAM-1)-harnessed SAINT-based lipid carrier system. *PLOS ONE* 10(9), e0138870 (2015).
35. Fang RH, Jiang Y, Fang JC, Zhang L. Cell membrane-derived nanomaterials for biomedical applications. *Biomaterials* 128, 69–83 (2017).

36. Wang Y, Zhang K, Li T *et al.* Macrophage membrane functionalized biomimetic nanoparticles for targeted anti-atherosclerosis applications. *Theranostics* 11(1), 164–180 (2021).

•• **Many methods in our study referred to this literature: based on macrophage 'homing' into atherosclerotic lesions and cell membrane coating nanotechnology, biomimetic nanoparticles were fabricated with a macrophage membrane coating on the surface of rapamycin-loaded poly(lactic-co-glycolic acid) copolymer nanoparticles.**

37. Li Y, Che J, Chang L *et al.* CD47- and integrin alpha4/beta1-comodified-macrophage-membrane-coated nanoparticles enable delivery of colchicine to atherosclerotic plaque. *Adv. Healthc. Mater.* 11(4), e2101788 (2022).

• **Many of the experimental methods referred to this literature: a modified-macrophage-membrane-coated nanoparticle drug delivery able to transport colchicine to the atherosclerotic site is reported.**

38. Zhuang J, Fang RH, Zhang L. Preparation of particulate polymeric therapeutics for medical applications. *Small Methods* 1(9), (2017).

39. Hu CM, Fang RH, Wang KC *et al.* Nanoparticle biointerfacing by platelet membrane cloaking. *Nature* 526(7571), 118–121 (2015).

40. Che J, Sun L, Shan J *et al.* Artificial lipids and macrophage membranes coassembled biomimetic nanovesicles for antibacterial treatment. *Small* 18(26), e2201280 (2022).

•• **For the important experimental methods of fusion membranes referred to in this reference: the fusion process of macrophage membranes and lipid membranes was determined using a fluorescence resonance energy transfer method.**

41. Pan T, Sun S, Chen Y *et al.* Immune effects of PI3K/Akt/HIF-1alpha-regulated glycolysis in polymorphonuclear neutrophils during sepsis. *Crit. Care* 26(1), 29 (2022).

42. Zhao J, Liu Z, Chang Z. Lipopolysaccharide induces vascular endothelial cell pyroptosis via the SP1/RCN2/ROS signaling pathway. *Eur. J. Cell Biol.* 100(4), 151164 (2021).

43. Dong X, Gao J, Zhang CY, Hayworth C, Frank M, Wang Z. Neutrophil membrane-derived nanovesicles alleviate inflammation to protect mouse brain injury from ischemic stroke. *ACS Nano* 13(2), 1272–1283 (2019).

44. Zhang Q, Dehaini D, Zhang Y *et al.* Neutrophil membrane-coated nanoparticles inhibit synovial inflammation and alleviate joint damage in inflammatory arthritis. *Nat. Nanotechnol.* 13(12), 1182–1190 (2018).

45. Park JH, Jiang Y, Zhou J *et al.* Genetically engineered cell membrane-coated nanoparticles for targeted delivery of dexamethasone to inflamed lungs. *Sci. Adv.* 7(25), (2021).

46. Arslan F, De Kleijn DP, Pasterkamp G. Innate immune signaling in cardiac ischemia. *Nat. Rev. Cardiol.* 8(5), 292–300 (2011).

47. Frantz S, Bauersachs J, Ertl G. Post-infarct remodelling: contribution of wound healing and inflammation. *Cardiovasc. Res.* 81(3), 474–481 (2009).

48. Frangogiannis NG. Regulation of the inflammatory response in cardiac repair. *Circ. Res.* 110(1), 159–173 (2012).

49. Sreejit G, Abdel-Latif A, Athmanathan B *et al.* Neutrophil-derived S100A8/A9 amplify granulopoiesis after myocardial infarction. *Circulation* 141(13), 1080–1094 (2020).

50. Jiang Q, Liu Y, Guo R *et al.* Erythrocyte-cancer hybrid membrane-camouflaged melanin nanoparticles for enhancing photothermal therapy efficacy in tumors. *Biomaterials* 192, 292–308 (2019).

51. Deanfield JE, Halcox JP, Rabelink TJ. Endothelial function and dysfunction: testing and clinical relevance. *Circulation* 115(10), 1285–1295 (2007).

52. Filippi MD. Neutrophil transendothelial migration: updates and new perspectives. *Blood* 133(20), 2149–2158 (2019).

53. Xu M, Qi Y, Liu G, Song Y, Jiang X, Du B. Size-dependent *in vivo* transport of nanoparticles: implications for delivery, targeting, and clearance. *ACS Nano* 17(21), 20825–20849 (2023).

54. Meyer RA, Sunshine JC, Green JJ. Biomimetic particles as therapeutics. *Trends Biotechnol.* 33(9), 514–524 (2015).

55. Han Y, Zhao R, Xu F. Neutrophil-based delivery systems for nanotherapeutics. *Small* 14(42), e1801674 (2018).

• **Much of the introduction and discussion of our article referred to this article: neutrophil-based delivery has shown great potential in circumventing nanotherapeutics limitations, such as low biocompatibility, short circulation time and immunogenicity of nanomaterials.**

56. Chae HJ, So HS, Chae SW *et al.* Sodium nitroprusside induces apoptosis of H9C2 cardiac muscle cells in a c-Jun N-terminal kinase-dependent manner. *Int. Immunopharmacol.* 1(5), 967–978 (2001).

57. Bonato JM, De Mattos BA, Oliveira DV, Milani H, Prickaerts J, De Oliveira RMW. Blood–brain barrier rescue by roflumilast after transient global cerebral ischemia in rats. *Neurotox. Res.* 41(4), 311–323 (2023).

58. Refaie MMM, Fouli Gaber Ibrahim M, Fawzy MA *et al.* Molecular mechanisms mediate roflumilast protective effect against isoprenaline-induced myocardial injury. *Immunopharmacol. Immunotoxicol.* 45(6), 650–662 (2023).